Load Reduction of Wind Turbines Using Receding Horizon Control

Mohsen Soltani, Rafael Wisniewski, Per Brath, and Stephen Boyd

Abstract— **Large scale wind turbines are lightly damped mechanical structures driven by wind that is constantly fluctuating. In this paper, we address the design of a model-based receding horizon control scheme to reduce the structural loads in the transmission system and the tower, as well as provide constant (or at least smooth) power generation. Our controller incorporates two optimization problems: one to predict or estimate mean wind speed, given LIDAR data, and the other to carry out receding horizon control to choose the control inputs. The method is verified against an existing wind turbine control system, and shows reductions in both extreme loads and power fluctuations by 80% and 90% respectively, when compared to a conventional controller.**

I. INTRODUCTION

The size of wind turbine structures has been increasing rapidly during the last decade. Consequently, modern wind turbines use lighter materials, which together with the expansion of the size result in a less stiff structure. When designing the wind turbine structure, one of the most challenging issues is to design a control system which is able to dampen the fluctuations of structural loads. The control of wind turbines differs from control of a generic mechanical system, since the source of the mechanical loads is the wind, which is also the source of the driving force of the turbine. In other words, this source comprises an uncontrollable input for the system.

In variable speed horizontal-axis wind turbines, the aerodynamic torque is controlled by pitching the blades in full load operation [1]. In addition, the generator torque is adjusted to specify the transmission torque. The pitch control is a conventional *gain-scheduled PID controller* acting on the generator speed. The reason that PID controllers are widely used in industry is that they have a simple structure and they can be easily tuned. However, their performance is not optimal. Hence, they are mostly used for small-scale turbines.

Modern wind turbines are equipped with advanced sensors such as strain gages, accelerometers, and recently light detection rnd ranging (LIDAR). With the use of these sensors more complex controllers are designed for further load reduction [2], [3], [4], [5]. In this paper, we demonstrate what can be gained when a LIDAR sensor is utilized. Using similar concept to radars, LIDAR is able to measure wind conditions such as speed and direction. When the LIDAR is mounted on the wind turbine, it is able to measure the wind speed at a distance in front of the wind turbine. For wind turbine control, this is of great importance when the coming wind is measured in advance, because the controller is able to optimize the operation for the time horizon in which the wind is measured. Consequently, *receding horizon control* (RHC) is chosen as a good candidate for wind turbine control when LIDAR data is available.

RHC has become popular during the last three decades. In RHC, we find the optimal inputs at each step in order to move the system states on an optimal path over a fixed time horizon. The solution of the current inputs will be applied to the system and the time horizon will be shifted forward to the next sample time. Such a controller is generally not optimal, but recent work on bounding controller performance has shown that it is often close to optimal [6]. The main drawback of RHC up until recently was the large computation time required in each step (since a full optimization problem is solved), which limited its use to slower systems, with sample rates measured in seconds (or longer). This problem has however been addressed in [7] and [6]. In these works, fast optimization methods are developed, that can solve the problems arising in RHC in times scales measured in milliseconds or even microseconds.

The dynamics of wind turbine systems are nonlinear, so the optimization problems arising in RHC are not convex. In this paper, we will see that the nonlinear dynamics of the wind turbine can be very well modeled as a linear parameter varying (LPV) model. The varying parameter is the mean wind speed, which is estimated using another optimization algorithm, from the LIDAR data. The estimation algorithm runs in a separate loop and provides the estimates for the RHC loop, which obtains the optimal control input for the receding horizon. In order to verify the method, we present some extreme load conditions and compare the performance of the RHC controller to the conventional PID controller with respect to load reduction and power fluctuations.

II. MODEL

A. Shaft and Tower Dynamics

The kinetic energy of the wind flowing into the rotor disc is given by

$$\Delta E = \frac{1}{2}\rho A \Delta X v_r^2, \tag{1}$$

where ρ is the air density, v_r is the average wind speed on the disc, A is the area of the disc, and $\Delta X = v_r \Delta t$ is the displacement of the air during the time interval Δt. Thus,

This work was supported by Vestas Wind Systems A/S.

Mohsen Soltani is with the Department of Electronics Systems, Aalborg University, 9220 Aalborg OE, Denmark sms@es.aau.dk

Rafael Wisniewski is professor at the Department of Electronics Systems, Aalborg University, 9220 Aalborg OE, Denmark raf@es.aau.dk

Per Brath is control specialist at Vestas Technology R&D, 8200 Arhus N, Denmark pebr@vestas.com

Stephen Boyd is professor at the Department of Electrical Engineering, Stanford University, 94305 Palo Alto, CA, USA boyd@stanford.edu

the total wind power corresponding to $\lim_{\Delta t \to 0} \Delta E/\Delta t$ will be

$$P = \frac{1}{2}\rho A v_r^3. \tag{2}$$

Wind turbine blades only transfer part of the kinetic energy of the wind flow into shaft mechanical energy. The obtained mechanical energy is highly dependent on the blade aerodynamic efficiency which is expressed by the power coefficient C_P. In wind turbine aerodynamics [8], there are two major variables that change C_P: the blade pitch angle β and the blade tip speed ratio $\lambda = R\omega_r/v_r$, where R is the radius of the rotor plane and ω_r is the rotor angular velocity. In fact, C_P is a function which is calculated by solving the blade element momentum equations [8]. The result of the numeric calculations are provided in a look-up table. Thus, the total absorbed mechanical power by the rotor is given by

$$P_r = \frac{\pi}{2}\rho R^2 v_r^3 C_P(\lambda, \beta). \tag{3}$$

The mechanical energy will exert a torque on the rotor which is

$$T_r = P_r/\omega_r = \frac{\pi}{2}\rho R^2 \frac{v_r^3}{\omega_r} C_P(\lambda, \beta). \tag{4}$$

Rotor torque will be transfered to the electrical generator through the gearbox. However, the gearbox and shafts are not stiff, i.e, the transmission system will also absorb some of the energy and convert it to the potential energy. In order to provide a model for the transmission system, we assume that the gearbox is a rigid body while transferring the deformations on the low-speed shaft. Fig. 1 shows the structural model of such a transmission system. The low-speed shaft is modeled by a rotational moment of inertia, a viscous damper and a viscously damped rotational spring. The inertia I_r represents the inertia of the rotor and shaft. The viscous damper, with damping constant B_r, models the bearings. The stiffness and damping of the rotor are K_θ and B_θ respectively. In this model, θ represents the shaft torsion. The high-speed shaft is modeled by a smaller inertia and a damper. The high-speed shaft is relatively stiff; and thus, we can neglect the spring in the right side. The rotational moment of inertia in the generator side, I_g represents the sum of inertia of the high-speed shaft, gearbox and the rotor of the generator. The viscous damper, with damping constant B_g, represents the viscosity of the high-speed shaft bearings.

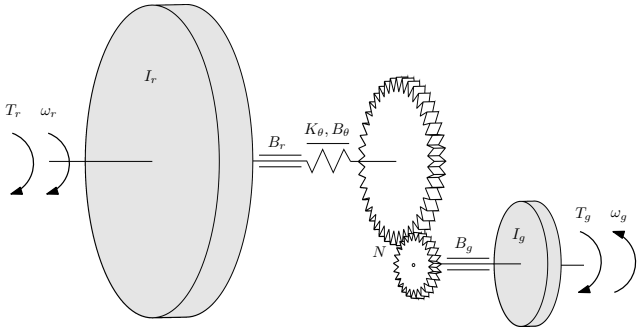

Fig. 1. Mechanical scheme of the wind turbine transmission system.

The mechanical model in Fig. 1 corresponds to the following differential equations

$$\begin{aligned} I_r\dot{\omega}_r &= T_r - K_\theta\theta - B_\theta\dot{\theta} - B_r\omega_r \\ I_g\dot{\omega}_g &= -T_g + \frac{K_\theta}{N}\theta + \frac{B_\theta}{N}\dot{\theta} - B_g\omega_g \\ \dot{\theta} &= \omega_r - \frac{\omega_g}{N}, \end{aligned} \tag{5}$$

where N is the gear ratio, ω_g is the generator angular velocity, and T_g is the generator torque.

In a *double-fed induction generator* (DFIG), the electric power is normally controlled by changing the rotor current, which results in changing the torque acting on the high-speed shaft. As a consequence, the generator torque is one of the control inputs for the wind turbine system. In summary, the produced electrical power P_e is obtained from the following differential equation

$$\dot{P}_e = \frac{1}{\tau_p}(T_g\omega_g - P_e), \tag{6}$$

where τ_p is the time constant.

The tower fore-aft deflection is the result of the wind force on the rotor, known as thrust force. We consider the kinetic energy in equation (1) and zero potential energy. The total force of the wind on the disc is given by the Lagrangian $L = \Delta E$ as

$$F = \frac{\partial L}{\partial \Delta X} - \frac{d}{dt}\frac{\partial L}{\partial \Delta \dot{X}}, \tag{7}$$

that is

$$F = \frac{1}{2}\rho A v_r^2. \tag{8}$$

Similar to the power calculation, the thrust force on the turbine blades is always less than the total force of the wind. This will again depend on the blade aerodynamics which is described by a dimensionless thrust coefficient C_T. The thrust coefficient is also a function of λ and β. In practice, $C_T(\lambda, \beta)$ is calculated by solving the blade element momentum theory equations. The result of the numeric calculations are provided in a look-up table. Consequently, the thrust force on the rotor is

$$F_t = \frac{\pi}{2}\rho R^2 v_r^2 C_T(\lambda, \beta). \tag{9}$$

Thrust force will be transfered to the tower top through the nacelle. This force will result on tower fore-aft motion. The tower is lightly damped structure due to its size and material, which is mostly steel. It is possible to simplify the tower fore-aft motion by a mass, spring, and damper model. Fig. 2 shows the schematic of this model. This schematics represent the dynamics of the tower fore-aft as follows

$$M_t\ddot{y} + B_t\dot{y} + K_t y = F_t, \tag{10}$$

where y is the tower top displacement, M_t, B_t, and K_t are the identified mass, damping coefficient, and stiffness for this model. The coefficients are approximated by finite elements.

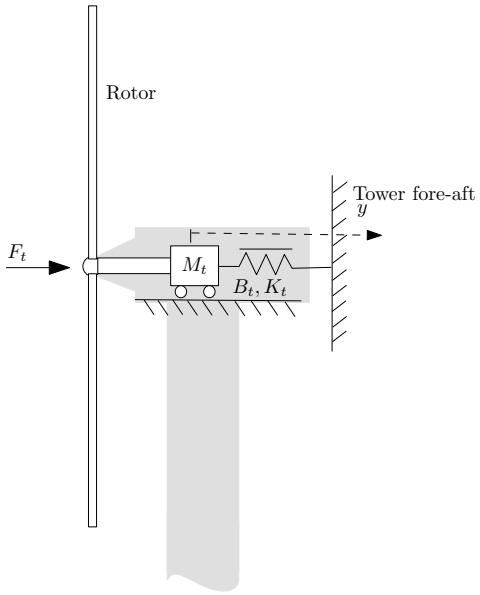

Fig. 2. Mechanical scheme of the wind turbine tower fore-aft motion.

B. Linearization

Equations (4, 5, 6, 9, and 10) form the governing nonlinear differential equations of the wind turbine model. We express these equations as

$$\dot{x}_n = f(x_n, u_n, v_r), \tag{11}$$

where $x_n = (\omega_r, \omega_g, \theta, y, \dot{y}, P_e)$ is the vector of wind turbine states, $u_n = (\beta, T_g)$ is the vector of the control inputs, and v is the average ambient wind speed on the rotor area. The functions $C_P(\lambda, \beta)$ and $C_T(\lambda, \beta)$ are given in lookup tables; however, we approximate them by differentiable functions by smoothing the edges. Thus, linearization of the model is possible using the first order term of Taylor approximation of (11) in the neighborhood of the operating points $(x_n^{*T}, u_n^{*T}, v_r^*)$, which are solutions of $f(x_n^*, u_n^*, v_r^*) = 0$. The wind turbine has to work in different wind speeds while wind speed is an uncontrollable input to the model. Thus, x_n^* and u_n^* are computed for different values of v^* in the operating range (which is usually between $4m/s$ to $25m/s$ for wind turbines). Consequently, the set of linear model equations can be expressed as follows

$$\dot{x} = A(\gamma)x + B(\gamma)u + D(\gamma)w, \tag{12}$$

where $x = x_n - x_n^*$, $u = u_n - u_n^*$, $w = v_r - v_r^*$, and γ is an estimation for the mean wind speed. The benefit of this formulation is that if changes of mean wind speed are slower than the system response, we will be able to stabilize the system using a parameter varying feedback. This requires establishing an algorithm which provides the mean wind speed.

C. Optimal Mean Wind Estimation

A moving average is traditionally used in the wind power industry in order to estimate the value of γ. This has a drawback of having a delayed estimate of γ. The delay does not cause a serious problem in turbulent wind as the deviation of the wind from the estimated operating point for wind is small (see Fig. 3a). However, we see a large deviation in the case of gust. Fig. 3b (red line) shows the estimated value of γ during a wind gust using the moving average. When the wind speed is at its peak of $19m/s$, the moving average shows the mean value of $13m/s$. Similarly, when the wind speed falls back to $13m/s$, the moving average is at its peak of $18m/s$. This deviation from the operating point results in a large model mismatch which causes high amount of loads as well as power fluctuations in such cases. A small window for the moving average will surely result in less delay; however, it will also result in fast variations of the varying parameter in the LPV system that might destabilize the closed-loop system, which was design under the assumption that γ changes slowly.

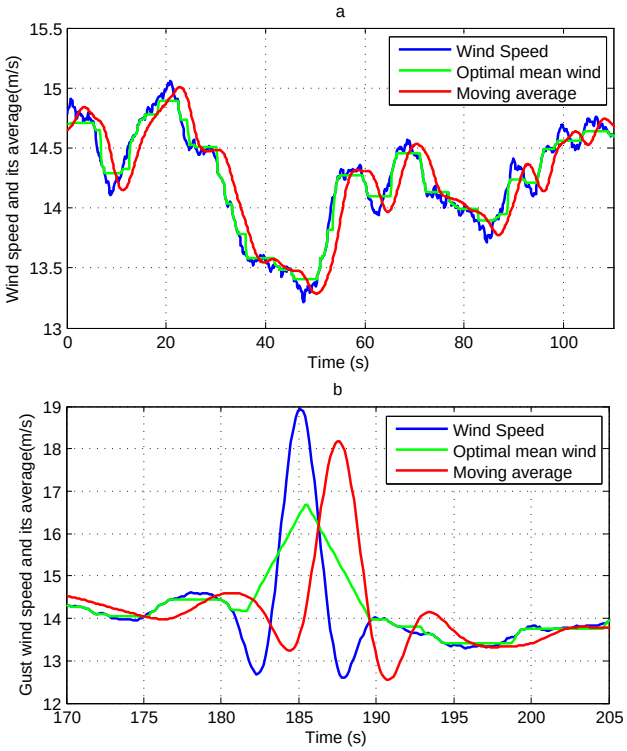

Fig. 3. Comparison of estimated mean wind speed using moving average and $\mathcal{L}_1$-regularized Least Square in (a) turbulent wind and (b) gust wind.

When LIDAR is used, we have the possibility to look at the wind in front of the turbine, and therefore, estimate the average wind speed without causing a delay. We benefit from the wind speed predictions and obtain the mean wind by solving an optimization problem. *Least squares* (LS) is the basic first choice to estimate the average values. However, it has a drawback; despite the low bias, the variation of the predictions are relatively high. The low bias may result in performance degradation; however, fast variations may destabilize the system. In order to avoid the fast variations we use LS estimation with *total variation* (TV) regularizaiton. Assume that the random variable $\hat{v}_k$ is available in the interval $(t_k, \ldots, t_{k+T_p})$. For known γ_{k-1}, the objective is to

find the values of γ_k in this interval that minimizes both mean square errors and variations in the rate of γ_k. Furthermore, we can limit the rate of the variation in γ_k by $\mathcal{S}$. This is interpreted as constraint in the following optimization problem

$$\begin{array}{ll} \text{minimize} & \sum_{j=k}^{k+T_p} (\hat{v}_j - \gamma_j)^2 + \lambda \sum_{j=k}^{k+T_p} |\gamma_j - \gamma_{j-1}| \\ \text{subject to} & |\gamma_j - \gamma_{j-1}| \leq T_s \mathcal{S}, \quad j = k, \ldots, k+T_p, \end{array} \tag{13}$$

with variables γ_j, where λ is the (positive) weight of the TV regularization and T_s is the sampling time. This problem is readily solved using, for example, an interior-point method in [9], [10].

Having the prediction of wind speed from LIDAR brings the possibility to use the future data in order to estimate the mean wind speed. It is not necessary to solve this optimization algorithm at each sampling time. In our implementation, we solve it for the second half of the predicted horizon. This means that we have $T_p T_s$ seconds to solve the problem, in which T_s is the sampling time and T_p is half the number of samples in prediction horizon. In case the number of samples is odd, we round T_p toward zero. Fig. 3-a,b show the result of the algorithm, when a prediction horizon of 5sec is used.

III. Receding Horizon Control

Equation (12) is a multivariable linear parameter varying (LPV) state-space equation. In receding horizon control, we need the current value of the states. Unfortunately, we are not able to measure all states. However, the states are observable. Thus, we measure the generator speed ω_g, tower deflection z, and electrical power P_e and employ a Luenberger observer to estimate the other states.

It is more convenient to use the discrete time representation of the model for receding horizon control. Thus, we express the discrete state-space model of equation (12) as

$$x_{k+1} = A_d(\gamma_k)x_k + B_d(\gamma_k)u_k + D_d(\gamma_k)w_k, \tag{14}$$

with $w_k = v_k - \gamma_k$. Most LIDARs provide the wind speed data at a distance in front of the turbine; however, for RHC we need a time history of the wind in front of turbine. This is achieved by assuming the turbulence to be frozen. We assume that the turbulent wind is moving toward the turbine with the speed of the average wind. Thus, in practice, we propagate the wind data in time in order to make a time history of the wind. To this end, the frozen turbulence assumption will result in uncertainties in wind information from LIDAR, $\hat{v}_k$, which is not exactly the same as v_k, and it includes the uncertainty e_k, i.e., $v_k = \hat{v}_k + e_k$. The prediction error e_k is assumed to be independent and identically distributed (IID) with known distribution for each k. Here, we assume that e_k has a normal distribution with zero mean and a standard deviation of about 10% of $\hat{w}_k$, where $\hat{w}_k = \hat{v}_k - \gamma_k$.

The objective function in RHC is defined as

$$J = \sum_{j=k}^{k+T-1} \ell(x_j, u_j) + \ell_f(x_{k+T}), \tag{15}$$

where T is the control horizon ($T < T_p$) and the function $\ell(x, u)$ is in the form

$$\ell(x_j, u_j) = \begin{bmatrix} x_j \\ u_j \end{bmatrix}^T \begin{bmatrix} Q & S \\ S^T & R \end{bmatrix} \begin{bmatrix} x_j \\ u_j \end{bmatrix} + q^T x_j + r^T u_j, \tag{16}$$

where Q and R are symmetric matricies with

$$\begin{bmatrix} Q & S \\ S^T & R \end{bmatrix}$$

positive semidefinite, and q and r are vectors of the same size as x and u. The function

$$\ell_f(x_{k+T}) = x_{k+T}^T Q_f x_{k+T} + q_f^T x_{k+T}$$

is used to emphasize a large penalty on the final cost. In RHC, the inputs have to be computed at each step by solving the following emphquadratic program (QP)

$$\begin{array}{ll} \text{minimize} & \sum_{j=k}^{k+T-1} \ell(x_j, u_j) + \ell_f(x_{k+T}) \\ \text{subject to} & x_{j+1} = A_d(\gamma)x_j + B_d(\gamma)u_j + D_d(\gamma)\hat{w}_j \\ & |u_{j+1} - u_j| \leq T_s u_s \\ & |u_j - 2u_{j-1} + u_{j-2}| \leq T_s^2 u_a \\ & j = k, ..., k+T-1 \end{array} \tag{17}$$

where the optimization variables are $x_{k+1}, \ldots, x_{k+T}$ and $u_k, \ldots, u_{k+T-1}$, u_s and u_a are the constraints on the inputs, e.g., pitch velocity and acceleration, and u_{k-1} and u_{k-2} are the inputs at the previous samples. Only the first computed input will be used at each time step. The convex optimization problem is solved using CVXGEN [11], [12], which generates a fast custom reliable solver which applies standard primal-dual interior point method to solve QPs.

The mean estimation and receding horizon control algorithms are implemented in two separate loops which runs in parallel. Assume that both loops start at time t_k, the algorithms are as following:

Mean wind estimation loop

1: Solve (13) for $j = k + T_p + 1, \ldots, k + 2T_p$ and obtain $\gamma_{k+T_p+1}, \ldots, \gamma_{k+2T_p}$.
2: Wait until sample $k + T_p + 1$.
3: $k \leftarrow k + T_p + 1$ and update the samples of $\hat{v}_k$.
4: Jump to 1.

RHC loop

1: Solve (17) for $j = k, \ldots, k+T$ and obtain $u_k, \ldots, u_{k+T}$.
2: Apply u_k to the inputs.
3: Wait until sample $k + 1$.
4: $k \leftarrow k + 1$ and update the variables x_k, $\hat{w}_k$, γ, u_{k-1}, and u_{k-2}.
5: Jump to 1.

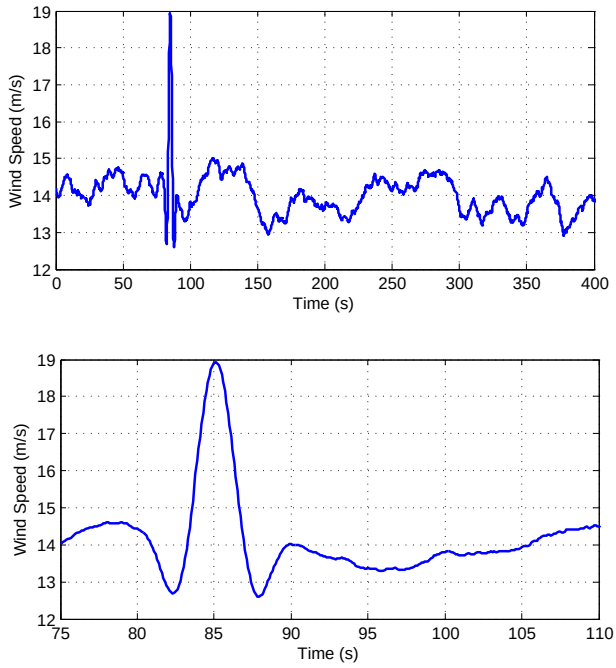

Fig. 4. Rotor wind speed with 50 year return gust (top figure), zoomed in to the gust interval (bottom figure).

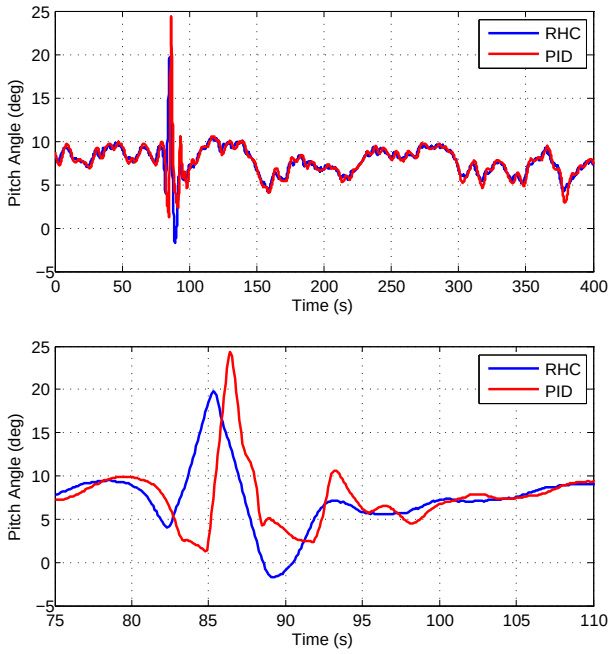

Fig. 5. Blade pitch angle (top figure), zoomed in to the gust interval (bottom figure).

IV. Results

The implemented RHC is verified against different extreme wind cases. The extreme wind evaluations show the worst case loads caused by the wind variation. The controller response to one of the most severe wind cases is demonstrated in this paper. According to IEC 6400-1 (see [8]), the gust speed with a return period of 50 years shall be taken in wind turbine certification tests. The wind is generated at the rotor disc by simulation of the wind speed spectrum and coherence for a given mean wind speed. The effective wind speed is achieved by averaging the point wind speed over the rotor disc. The gust is added to the wind speed. The shape of the gust ('rising and falling gust') is the well-known Mexican-hat function which incorporates slight fall before and after rising by

$$v(h,t)=\begin{cases} V(h)-0.37V_{gust}\sin(\frac{3\pi t}{T_s})(1-\cos(\frac{2\pi t}{T_s})) & t_s\leq t\leq t_s+T_s \\ V(h) & \text{otherwise} \end{cases} \tag{18}$$

where $V(h)$ is the mean wind speed at height h, t_s is start of the gust and T_s is its duration, and V_{gust} is the amplitude defined by

$$V_{gust}=\frac{6.4\sigma_u}{1+0.2\frac{R}{\Lambda}}, \tag{19}$$

where σ_u is the standard deviation of the turbulent wind fluctuations and Λ is the turbulence scale parameter [8].

Fig. 4 shows the wind speed with incorporated gust of $10s$ duration. A prediction horizon of $4s$ seconds is used for estimation of mean wind speed while the optimization problem (13) is solved in a fraction of a second. The control horizon of 10 samples with sampling time of $0.15s$ is used. The RHC solver CVXGEN is able to provide the solution for (17) in $5ms$ (using Core Duo CPU @ 2.5GHz under Windows 7). The collective pitch angle is illustrated in Fig. 5 in which we compare two control strategies in the designed load case; RHC (blue line) and conventional gain-scheduled PID control (red line). Most methods of wind turbine control which focus on reduction of structural loads have a drawback of increasing the pitch activity. Since we have introduced a cost on variations of u in the optimization objective (16), the overall pitch activity remains at the same level in RHC case. Fig. 5-bottom shows a phase difference between RHC and PID control. The reason for this difference is the use of wind speed prediction in RHC. During large variations of wind speed, RHC is clearly prepared for reaction in advance, and thus, it will improve the performance by choosing the optimal path. Fig. 6 shows the reduction of about 88% in fluctuations of power when we used the RHC. In like manner, Fig. 7 shows the reduction of about 80% in magnitude of the fluctuations in tower top fore-aft deflection. Fig. 8 shows the reduction of about 82% in magnitude of the fluctuations in main shaft torsion when using RHC.

V. Conclusion

In this paper, we addressed the design of a receding horizon controller for a wind turbine. The control system solved an optimization problem in a time horizon in which the wind was predicted using LIDAR sensor. The linearization of wind turbine model led to a linear parameter varying system, which takes the mean wind speed as an input variable in order to determine the future response of the system. The estimation of mean wind was improved using an estimator. Subsequently, the result was used in a RHC scheme which provided the optimal control inputs for a

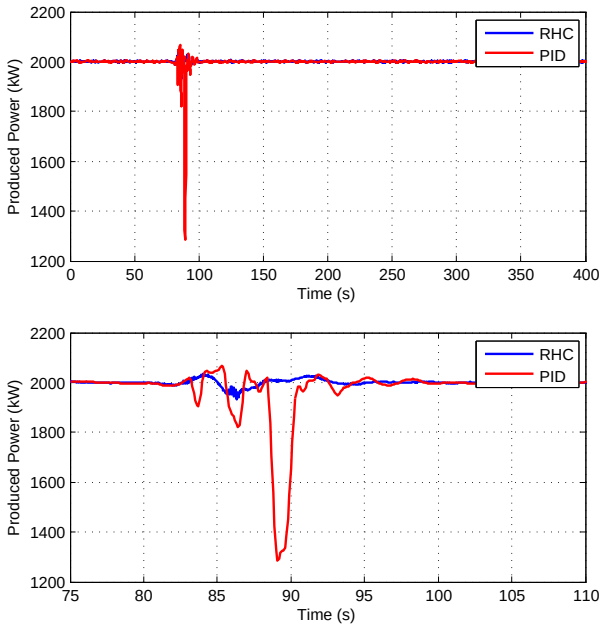

Fig. 6. Produced electrical power (top figure), zoomed in to the gust interval (bottom figure).

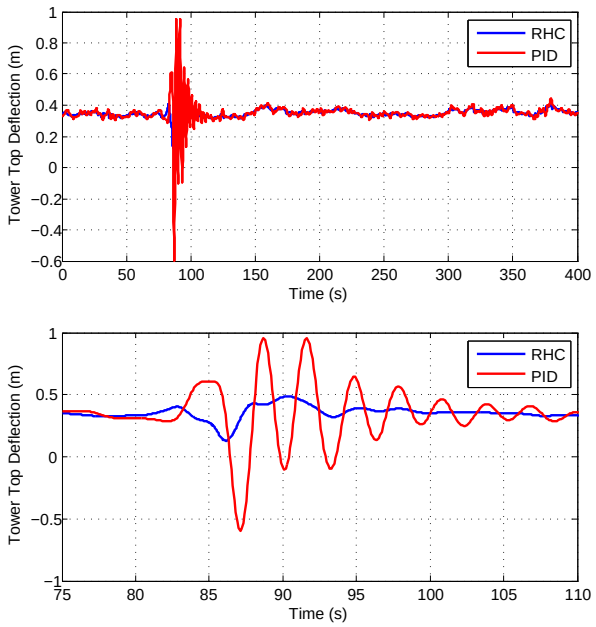

Fig. 7. Tower top deflection in fore-aft direction (top figure), zoomed in to the gust interval (bottom figure).

fixed control horizon. Finally, RHC was compared to the conventionally used PID control in extreme wind conditions. The results showed significant reduction in structural loads as well as improvements in output power fluctuations.

REFERENCES

[1] E. A. Bossanyi, "Wind turbine control for load reduction," *Wind Energy*, vol. 6, pp. 229–244, 2003.

[2] C. Bottasso and A. Croce, "Cascading kalman observers of structural flexible and wind states for wind turbine control," Tech. Rep., 2009.

[3] E. A. Bossanyi, "Further load reduction with individual pitch control," *Wind Energy*, vol. 8, pp. 481–485, 2005.

[4] W. Leithead, V. Neilson, S. Dominguez, and A. Dutka, "A novel approach to structural load control using intelligent actuators," in *17th Mediterranean Conference on Control and Automation*, Jun. 2009, pp. 1257–1262.

[5] T. J. Larsen, H. A. Madsen, and K. Thomasen, "Active load reduction using individual pitch, based on local in flow measurements," *Wind Energy*, vol. 8, 2005.

[6] Y. Wang and S. Boyd, "Fast model predictive control using online optimization," *IEEE Transactions on Control Systems Technology*, vol. 18, no. 2, pp. 267–278, Mar. 2010.

[7] J. Mattingley, Y. Wang, and S. Boyd, "Code generation for receding horizon control," in *IEEE International Symposium on Computer-Aided Control System Design (CACSD)*, Sep. 2010, pp. 985–992.

[8] T. Burton, D. Sharpe, N. Jenkins, and E. Bossanyi, *Wind Energy Handbook*. John Wiley, 2008.

[9] S. Boyd and L. Vandenberghe, *Convex Optimization*. Cambridge University Press, 2004.

[10] S. J. Kim, K. Koh, M. Lustig, S. Boyd, and D. Gorinevsky, "An interior-point method for large-scale l1-regularized least squares," *IEEE Journal on Selected Topics in Signal Processing*, vol. 1, no. 4, pp. 606–617, Dec. 2007.

[11] J. Mattingley and S. Boyd, "Real-time convex optimization in signal processing," *IEEE Signal Processing Magazine*, vol. 27, no. 3, pp. 50–61, May 2010.

[12] ——, "Cvxgen: A code generator for embedded convex optimization," Nov. 2010. [Online]. Available: http://www.stanford.edu/boyd/papers/code_gen_impl.html

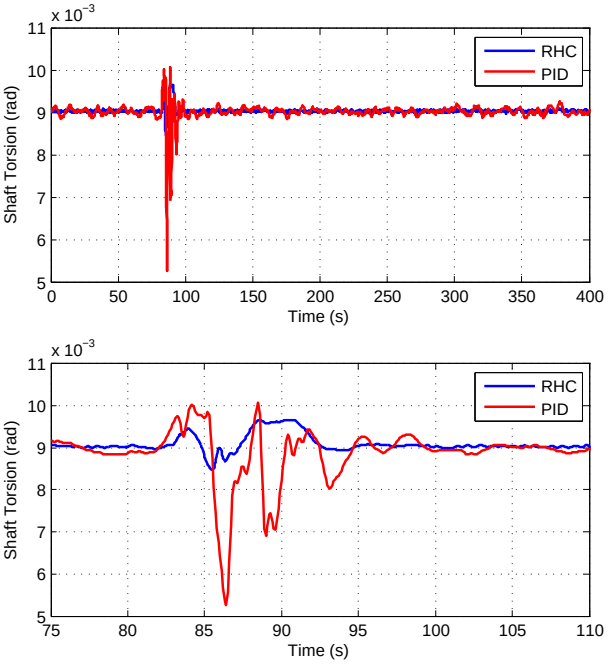

Fig. 8. Main shaft torsion (top figure), zoomed in to the gust interval (bottom figure).